William & Mary
CHARTERED 1693

W&M ScholarWorks

Arts & Sciences Articles

Arts and Sciences

6-2-2018

Low-cost wave characterization modules for oil spill response

E. D. Skinner
College of William and Mary

M. M. Rooney
College of William and Mary

Mark K. Hinders
College of William and Mary, hinders@wm.edu

Follow this and additional works at: https://scholarworks.wm.edu/aspubs

Recommended Citation

Skinner, E. D.; Rooney, M. M.; and Hinders, M. K., "Low-cost wave characterization modules for oil spill response" (2018). JOURNAL OF OCEAN ENGINEERING AND SCIENCE. 31. 96-108. 10.1016/j.joes.2018.05.003

This Article is brought to you for free and open access by the Arts and Sciences at W&M ScholarWorks. It has been accepted for inclusion in Arts & Sciences Articles by an authorized administrator of W&M ScholarWorks. For more information, please contact scholarworks@wm.edu.

Available online at www.sciencedirect.com

ScienceDirect

Journal of Ocean Engineering and Science 3 (2018) 96–108

www.elsevier.com/locate/joes

Original Article

Low-cost wave characterization modules for oil spill response

E.D. Skinner, M.M. Rooney, M.K. Hinders*

Department of Applied Science, William & Mary, Williamsburg, VA 23187-8795, United States

Received 22 January 2018; accepted 7 May 2018
Available online 8 June 2018

Abstract

Marine oil spills can be remediated by mechanical skimmers in calm waters, but performance degrades with increased wave height. We have developed and demonstrated a system that quantifies local wave characteristics with an uncertainty of four inches of heave. Our system is intended for the measurement of wave characteristics during oil spill recovery. It conveys this information to coordinators and responders in real time via WiFi and remote reporting through a satellite network. This information will allow for enhanced situational awareness during an oil spill response, assisting stakeholders and optimizing mechanical skimming operations. Our wave characterization module (WCM) uses accelerometer outputs from a very small inertial measurement unit (IMU) to generate wave statistics and calculate wave characteristics. It is configured such that a WCM can either be attached to a skimmer float or incorporated into a microbuoy. Wave height and period are transmitted via WiFi and/or a satellite-enabled mesh-grid network to a cloud-hosted geographic information system (GIS). Here, we discuss the bare-bones sensors-plus-algorithm approach we developed by using spring-mass systems to approximate the wave height and period regime of interest. We then describe open water tests carried out using that development system both mounted to a weir skimmer mockup and packaged in a microbuoy. Finally, we present controlled tests in the wave tank at Ohmsett, the National Oil Spill Response Test Facility in New Jersey, with the WCMs communicating the wave characteristics via WiFi to tankside laptops and via satellite to the cloud-based GIS. Snapshot determinations of wave height calculated using the scalar magnitude of the three-axis accelerometer in the IMU were within four inches of the benchmark wave measurement system at Ohmsett.

© 2018 Shanghai Jiaotong University.
This is an open access article under the CC BY-NC-ND license. (http://creativecommons.org/licenses/by-nc-nd/4.0/)

Keywords: Oil spill; Wave characterization module; Inertial measurement unit; Microbuoy.

1. Introduction

Marine oil spills can rapidly be contained by booms and remediated by mechanical skimmers. However, these are most effective in calm waters [1] with performance dropping off with increased wave height and decreased wave period [2,3]. Although much of this technology is mature, a variety of research is underway to develop and evaluate improved oil recovery technology [4,5]. Legacy sea-state monitoring systems with large discrete instrumentation packages provide decades of work refining algorithms which interpret sensor output that can be effectively leveraged.

There are a number of free-form buoy devices available on the market that have various sensors and communicate their data remotely. The iSphere and Argosphere communicate both their location and the sea surface temperature [6]. Buoys with wave characterization capabilities include the Seawatch Buoys from Fugro OCEANOR [7], the Waverider buoys from Datawell BV [8], and the TRIAXYS buoys from AXYS Technologies [9]. The TRIAXYS g3 Wave Sensor provides numerous wave parameters and typical wave statistics features. The majority of these buoys are over 0.5 m in diameter and employ moorings, requiring special equipment to deploy. The Mini Directional Waverider GPS by Datawell [10] has the capacity for satellite communication and uses GPS to characterize wave movements. As they are highly sensitive to lateral movement, these buoys require an additional external antenna to determine wave height accurately. A recent review of measurement platforms for sea surface elevation, especially

* Corresponding author.
E-mail address: hinders@wm.edu (M.K. Hinders).

https://doi.org/10.1016/j.joes.2018.05.003
2468-0133/© 2018 Shanghai Jiaotong University. This is an open access article under the CC BY-NC-ND license.
(http://creativecommons.org/licenses/by-nc-nd/4.0/)

accelerometer buoys, can be found in [11], and in [12], eleven platforms for measurement of spectral wave parameters are compared. There is also work underway around the world to develop small buoys for measurement of wave characteristics [13,14] and tracking oil spills [15,16] using GPS and satellite communication.

Wearables are the current leading edge of the Internet of Things with an increased emphasis on battery-charge life despite the imperative to include more sensing capability. The key enablers are tiny, low-power sensor hubs which fuse the inputs of several different types of microelectromechanical systems (MEMS) sensors, such as accelerometers, gyroscopes, and magnetometers, all without engaging the main processor and thereby reducing power consumption by up to 95%. This recent proliferation of highly capable, but small and low power, MEMS sensor hubs now makes it feasible to implement a very low cost WCM for buoys, skimmers, booms and the like in order to provide highly accurate and hyper-localized measurements of wave characteristics in real time during oil spill remediation.

The goal of our work was to develop a system that quantifies local wave characteristics with an uncertainty of four inches of heave. Our system is intended for the measurement of wave characteristics during oil spill recovery. It conveys this information to coordinators and responders in real time via WiFi and remote reporting through a satellite network. This information will allow for enhanced situational awareness during an oil spill response, assisting stakeholders and optimizing mechanical skimming operations.

Previous work has created a family of devices and applications based on a successful geo-referencing identification (GRID) tagging system for the autonomous and long-term global tracking of remote assets without the need for local infrastructure [17]. The WCMs described here augmented the latest generation of these GRID and satellite-enabled GRID (GRIDSAT) tags with integrated IMUs, containing three-axis accelerometers to measure wave characteristics, and associated microcontroller units (MCUs), with wave characterization algorithms to record, interpret and report wave data. The WCMs are designed to be mounted on commercially available mechanical skimmers to measure wave characteristics during oil spill response and recovery operations, providing quantitative feedback to operators and stakeholders.

The WCM uses accelerometer outputs from a very small IMU to calculate wave statistics, and is configured such that a WCM can be either attached to a skimmer float or incorporated into a microbuoy. Wave height and period are transmitted via WiFi and/or a satellite-enabled mesh-grid network to a cloud-hosted geographic information system (GIS). In this paper, we discuss the bare-bones sensors-plus-algorithm approach we developed by using spring-mass systems which approximate the wave height and period regime of interest. We then describe open water tests carried out using that development system both mounted to a weir skimmer mockup and packaged in a microbuoy. Finally, we present controlled tests in the wave tank at Ohmsett with the WCMs communicating the wave characteristics via WiFi to tankside laptops and via satellite to the cloud-based GIS. Snapshot determinations of wave height calculated using the scalar magnitude of the three-axis accelerometer in the IMU were within four inches of the benchmark wave measurement system at Ohmsett.

2. Algorithm development

2.1. Wave characterization

An ocean wave is a flow of energy traveling from its source, carried by the water. Therefore, anything floating on top of a wave, such as a buoy, moves in an elliptical rise-and-fall pattern [18]. This allows us to measure wave elevation from the surface of the ocean. A WCM-Buoy or WCM attached to a skimmer floating on the ocean's surface can be equipped with an accelerometer to measure its movement from crest to trough, which corresponds to the same movement of the wave at that particular point.

The sea surface is a superposition of waves of varying heights and periods moving in differing directions. Although simple sinusoidal motions can be readily analyzed by elementary methods, their regularity does not approximate the variability of ocean waves. When the wind blows and the waves swell in response, a wide range of heights and periods is developed, so at a fixed location in the ocean, the wave signals that a WCM outputs will be irregular. Though individual waves could be identified, there will always be significant variability in height and period from wave to wave. Thus, it is necessary to treat the characteristics of the sea surface in statistical terms [19–24].

We employ a modern machine-learning approach to ensure that the WCM can accurately output wave height for a variety of real-world situations. In some cases, like simple swell, the basic wave parameters would be straightforward to extract from the IMU sensor data. However, once the WCM is attached to a piece of equipment, the actual motion will be modified by the interaction of that equipment with the wave. This means that somewhat different IMU signal features need to be exploited, but a machine-learning approach is sufficiently robust to accommodate this. Moreover, we can also interpret complex wave fields where a simple one-dimensional wave model would fail. Rather than specifying IMU signal features that correlate with simple wave properties *a priori*, our approach is to train the algorithms with mockup and open-water wave data and then load the optimal feature set into the firmware. This will allow new situations and equipment to be incorporated in the future without modifying the WCM hardware.

The ocean surface is composed of a combination of wave components individually generated by the wind in different regions of the ocean propagating to the point of observation. Complex wave distributions are difficult to obtain in explicit form from a random wave model, but numerical algorithms based on the regression approximation work well. This method of calculating wave distributions is the only known method that gives correct answers valid for general spectra. We selected the Wave Analysis for Fatigue and Oceanogra-

phy (WAFO) toolbox, a third-generation package of MATLAB routines for statistical analysis and simulation of random waves, to calculate the distributions of wave characteristics from observed power spectra of the sea as measured by the WCM. WAFO provides a comprehensive set of validated computational tools for statistical analysis of random waves and a marine structure's responses to them [25]. In a random wave model, the distribution of wave characteristics, such as wave period and crest-trough wave height, can be calculated with high accuracy for almost any spectral type.

Through decades of time-series measurements of natural sea states, some statistical estimates of simple parameters have become standard in the literature. See, for example, Part II, Chapter 1 of the Coastal Engineering Manual (CEM), published by the United States Army Corps of Engineers' Coastal and Hydraulics Laboratory as posted by the University of California, San Diego [26]. The most important of these parameters is the significant wave height, Hsig, which is the mean of the largest third of waves recorded during the sampling period. This statistical measure corresponds to the wave height estimates made by experienced observers, because humans do not notice all of the small waves that pass by, but rather focus on the larger, more noticeable peaks. Since ocean conditions are constantly changing, measurements like significant wave height are necessarily short-term statistics calculated for time windows of approximately half an hour. Other wave parameters like average wave period can also be used to describe natural sea states, but these basic wave features ultimately give limited information about wave characteristics and behavior. Fortunately, physical oceanographers have developed analysis methods that give appropriately complete measures of ocean waves. From the CEM:

> "Mathematically, spectral analysis is based on the Fourier transform of the sea surface. The Fourier transform allows any continuous, zero-mean signal—like a time-series record of the sea surface elevation—to be transformed into a summation of simple sine waves. These sine waves are the components of the sea state, each with a distinct height, frequency, and direction. In other words, the spectral analysis method determines the distribution of wave energy and average statistics for each wave frequency by converting the time series of the wave record into a wave spectrum. This is essentially a transformation from the time-domain to the frequency-domain, and is accomplished most conveniently using a mathematical tool known as the Fast Fourier Transform (FFT).
>
> The spectral approach indicates what frequencies have significant energy content, as well as the direction wave energy is moving at each frequency. A wave spectrum can readily be plotted in a frequency vs. energy density graph, which can provide important information about a wave sample and the corresponding ocean conditions."

To determine the wave characterization information sent to the user, the WCM uses the onboard IMU and sensor MCU to record and process the raw data. The IMU reports the acceleration and angular velocity at a sufficiently high sampling rate to reconstruct the wave motion. During our initial laboratory and field-testing, we found that the majority of the motion of the WCM is vertical heave motion. This allowed us to simplify the displacement calculation by using the scalar magnitude of the three-axis accelerometer data instead of performing lengthy vector calculations using the gyroscope data. To calculate heave from the accelerometer data, we used a Fast Fourier Transform (FFT) to convert the data from the time domain into the frequency domain. We then filtered the data to isolate the wave frequencies of interest and calculated the wave period in seconds. We divided the frequency-domain signal by the frequency squared, and performed an Inverse Fast Fourier Transform (IFFT) to convert the data back to the time domain. We used this time-domain heave data with WAFO to run the spectral and statistical analysis to extract wave characteristics.

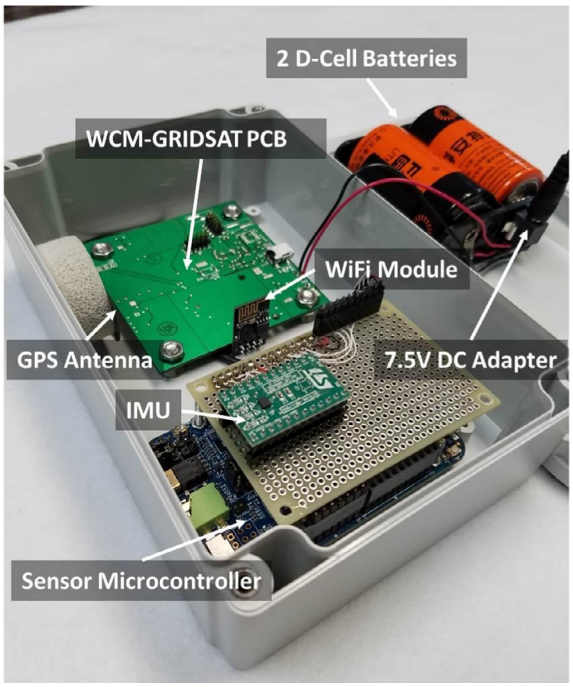

Fig. 1. WCM-embedded software development platform used for algorithm development and testing, provided by Evigia Systems, Inc. of Ann Arbor, MI. Evigia fabricated several pre-prototype WCMs for embedded software development and component testing, including WiFi and Bluetooth versions for further local wireless communication evaluation, testing the wireless protocols and data transfer via tablets and laptops. The most important enabler from the embedded software development platform was the ability to stream raw data from the IMU to develop and refine the wave characterization algorithms in parallel with the full design and fabrication of the WCM, WCM-Sat, and WCM-Buoy.

2.2. Laboratory testing

Testing was carried out with several different IMUs, including the WCM-embedded software development platform, shown in Fig. 1. We took systematic measurements first in the lab and then in the field to refine and optimize algorithms for the WCM platform. We mounted the sensors on several

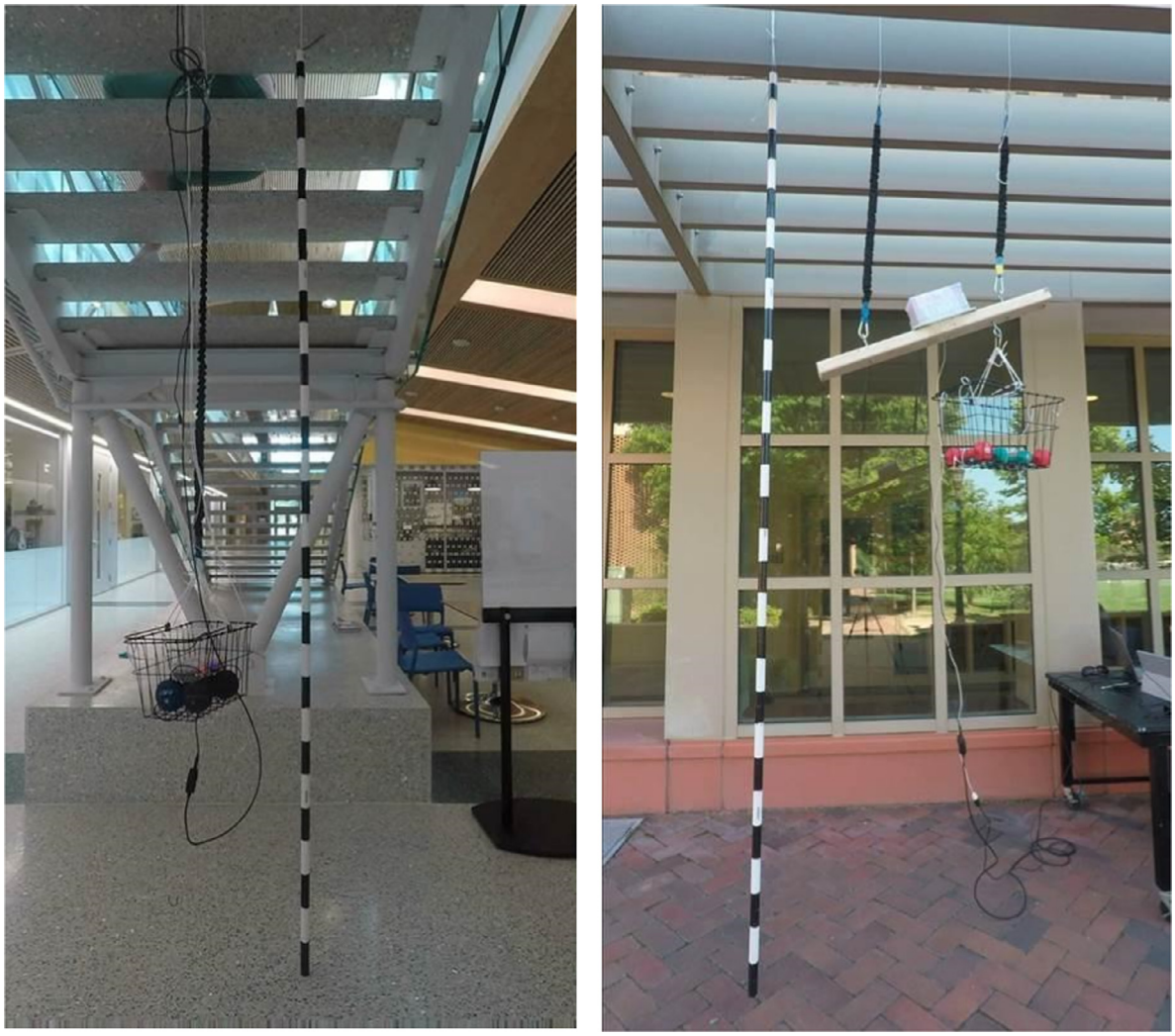

Fig. 2. Experimental setup using spring–mass combinations for algorithm development and verification. The hanging witness pole has markings every four inches, which was our performance objective.

spring–mass combinations to simulate ocean wave motions in a controlled laboratory environment. Carefully chosen spring–mass combinations gave displacements and frequencies approximating ocean waves in the region where it becomes necessary to decide whether to skim or disperse the oil. We released the sensors from varying heights and allowed the system to oscillate until little motion was evident.

We began testing with simple harmonic motion, using a single weighted spring setup to collect data. The photograph on the left in Fig. 2 shows that mockup apparatus with the WCM mounted in a weighted basket suspended by a single spring. We released the basket from a variety of heights and recorded the motion with both the IMU and a GoPro camera. The GoPro videos allowed us to note the peaks and troughs of the WCM's movement, which we estimated using the witness pole hanging alongside the spring–mass system. The witness pole was marked with four-inch bands to facilitate visual data collection. This visual data was compared to the IMU data to gauge the accuracy of the WCM's heave calculations.

Once we were convinced that the heave calculations for the simple harmonic motion were consistent with the physical heave, we progressed to a somewhat more complex experiment. We used combinations of springs and fixtures that produced multi-frequency responses, as one would expect in actual wave conditions. The photograph on the right in Fig. 2 shows an example of a mockup apparatus that gave multi-component oscillations. Here, we mounted the WCM on the weighted board suspended by a spring on either side. Varying both the weight and position of the basket as well as the mounting locations of the springs allowed us to collect a variety of data containing complex wave motion. Again, our visual data from the GoPro was compared to the IMU calculations.

Our laboratory testing confirmed that we could accurately calculate the heave motion of both simple harmonic and complicated multiple-frequency motion. Calculating displacement using the scalar magnitude of raw three-axis accelerometer data gave a close approximation of the heave. This enabled us to simplify the algorithm and remove the need to record

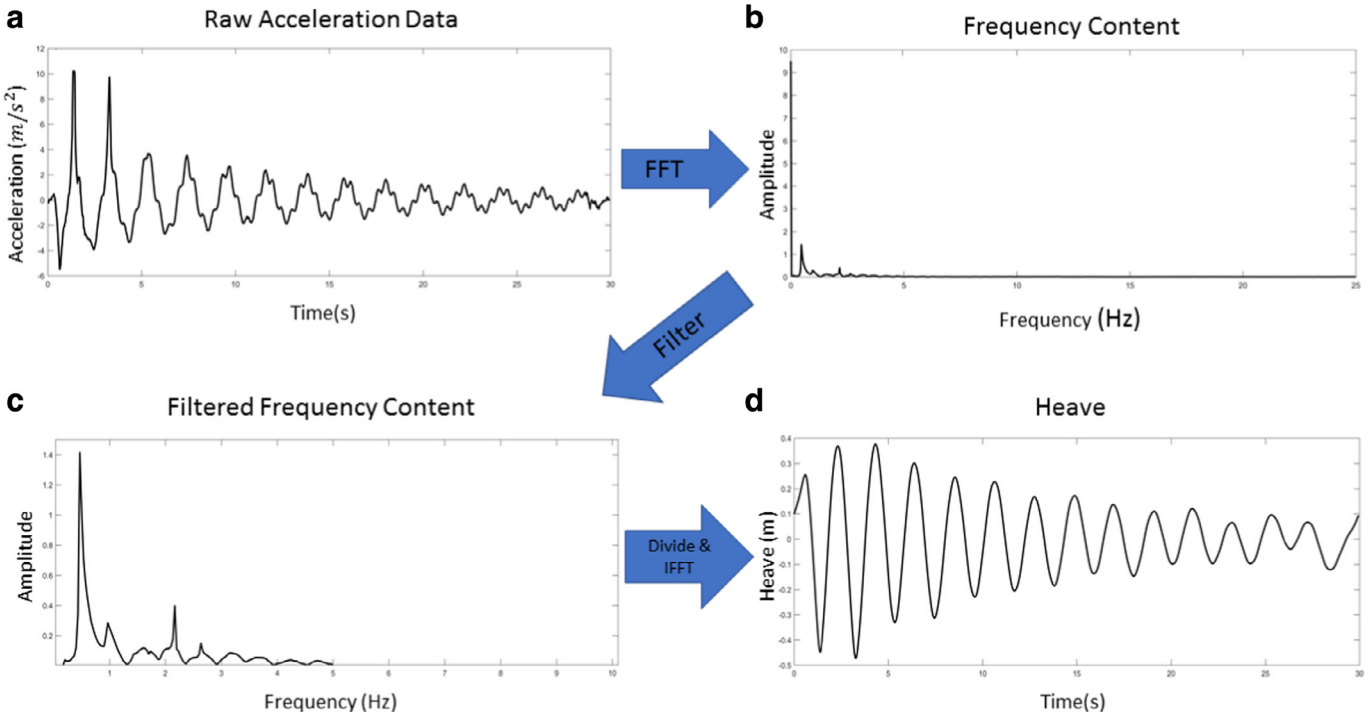

Fig. 3. Plots of wave characterization algorithm steps from acceleration to heave.

relatively battery- and memory-hungry gyroscope data, and to ensure that WCM output will not be sensitive to the orientation at which the device is mounted to oil spill recovery equipment.

Fig. 3 illustrates the steps in the bare-bones algorithm used to determine the heave of the WCM. For this test, we identified the maximum displacement as approximately 35 inches (0.9 m) from still frames of the GoPro video. Fig. 3(a) shows the raw z-axis accelerometer data, and Fig. 3(b) shows the resulting frequency spectrum after taking an FFT of the data. The frequency data was then filtered to isolate the wave frequencies and remove noise, as shown in Fig. 3(c). We divided the filtered data by the frequency squared and an IFFT was taken to create the plot of the heave, displayed in Fig. 3(d). According to the algorithm, the maximum height was approximately 15 inches (0.39 m) and the minimum height was approximately −19 inches (0.49 m), combining for a total displacement of about 34 inches (0.88 m). This gives a one-inch difference compared to the displacement noted visually during data acquisition.

We used the WAFO software for MATLAB to run the standard ocean wave spectral analysis and statistics on the heave data to calculate wave characteristics for the end user. Once the MATLAB algorithms were finalized, they were converted to C code and programmed on the sensor MCU. Using the scalar magnitude of the acceleration removed the need to store gyroscope data on the MCU, allowing for a higher sampling rate and longer data collection period on the final device.

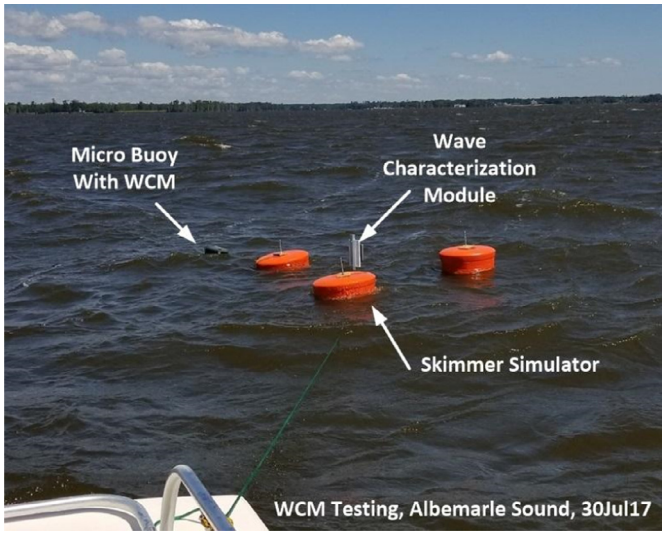

Fig. 4. Open water testing in Albemarle Sound, NC.

2.3. Open water testing: Albemarle Sound

To collect open-water data for refining the wave characterization algorithms, we built a mockup weir skimmer, shown in Fig. 4. The skimmer mockup approximated the buoyancy and dynamics of a typical weir skimmer, both in terms of the float geometry and the weight. The mockup weir skimmer was built from modular square tubing to provide a range of attachment points for WCMs. During testing, we attached buckets/sandbags filled with local sand to approximate the total weight of a real skimmer.

Fig. 5. Skimmer and two WCM-Buoy deployments looking down from the auxiliary bridge.

A second embedded software development platform was placed inside a buoy for streaming data collection over WiFi to compare results. The deployed testing setup is shown in Fig. 4. We positioned a witness pole in the water near the skimmer mockup and periodically recorded the wave height while streaming raw data to the boat from both the skimmer and buoy. Although there was some uncertainty in our observations using the witness pole, the calculated significant wave heights were within the four-inch performance objective.

3. Ohmsett testing and analysis

Each piece of the system architecture, including the embedded software development platform, message emulators to the WCM, satellite-enabled WCM (WCM-Sat), and WCM-Buoy, mesh networking, and local and remote reporting were unit tested and system tested to establish the accuracy of the reported data. The open-water tests on the Albemarle Sound were used to refine the wave characterization algorithms prior to conducting full WCM system testing at Ohmsett in Leonardo, NJ from September 5, 2017 through September 8, 2017 [27].

3.1. Facility and equipment setup and configuration

The Ohmsett wave tank is 203 m long, 20 m wide, and 3.5 m deep, and is capable of creating sine waves up to one meter high and simulating harbor chop waves [29]. Waves are generated by varying the stroke length (inches) of the hydraulic arms and the cycles per minute (CPM) of the stroke movement. WCMs, WCM-Sats, and embedded development platforms were secured to vertical brackets attached to a round plate mounted on a Desmi Terminator [30] weir skimmer float provided by Ohmsett, as shown in Fig. 5.

After being lowered into the water, the skimmer and WCM-Buoys were secured to the main bridge to prevent excessive drift from the testing area located between the main and auxiliary bridges. Altimeter Banner sensors extended over the water were used to measure the distance to the water's surface [28], and a MATLAB program was used to calculate significant wave height, wavelength, and period from the Banner data. One of the auxiliary bridge sensors is shown in Fig. 5. Table 1 summarizes the wave conditions for all the tests performed at Ohmsett.

Table 1
Ohmsett wave settings summary.

Test no.	Date	Start time	Stroke (inches)	CPM	Wave type
1	9/5	1:00 p.m.	18.0	18.0	Sine
2	9/5	2:00 p.m.	18.0	20.0	Sine
3	9/5	2:52 p.m.	7.5	35.0	Sine
4	9/5	3:30 p.m.	7.5	35.0	Sine
5	9/6	10:44 a.m.	18.0	18.0	Sine
6	9/6	11:23 a.m.	18.0	18.0	Sine
7	9/6	12:00 p.m.	18.0	20.0	Sine
8	9/6	2:45 p.m.	12.0	30.0	Sine
9	9/6	3:33 p.m.	12.0	30.0	Sine
10	9/6	4:03 p.m.	6.0	40.0	Sine
11	9/7	12:10 p.m.	6.0	40.0	Sine
12	9/7	12:53 p.m.	12.0	30.0	Chop
13	9/7	2:48 p.m.	12.0	30.0	Chop
14	9/7	3:33 p.m.	3.0	35.0	Chop
15	9/7	4:01 p.m.	3.0	35.0	Chop
16	9/8	9:10 a.m.	15.0	20.0	Chop
17	9/8	10:02 a.m.	18.0	10.0	Sine
18	9/8	10:22 a.m.	4.5	35.0	Sine
19	9/8	10:46 a.m.	12.0	25.0	Sine (Oil applied)
20	9/8	11:46 a.m.	7.5	35.0	Sine (Advancing)
21	9/8	1:10 p.m.	12.0	30.0	Sine
22	9/8	1:37 p.m.	18.0	18.0	Sine

3.2. Data collection and analysis

Each WCM device measured and reported wave characterization data. The embedded software development platform, mounted to the skimmer and contained in a buoy, streamed one minute of raw data during each data collection time window. The WCM, WCM-Sat, and WCM-Buoy each calculated and reported wave height, wave length, and wave period. The data transmitted from each device via WiFi were displayed on an iPad, stored on local memory and exported via email in comma-separated value files with the option of a dashboard screenshot. Data transmitted from the WCM-Sat and WCM-Buoy via satellite were stored in a MongoDB database and displayed on the GIS user interface. The raw gateway log was saved to a text file with a unique URL accessible via the Internet [27].

The WCM reports sea-state features of significant wave height, period, and wavelength to the end user. These features are determined using one minute of three-axis acceleration data to compute the surface elevation of the sea. We perform statistical analysis on the surface elevation, using the MATLAB WAFO software toolbox for analyzing waves [25], to calculate the sea-state features.

Significant wave height refers to the average wave height as it would be estimated by the human eye [19], his-

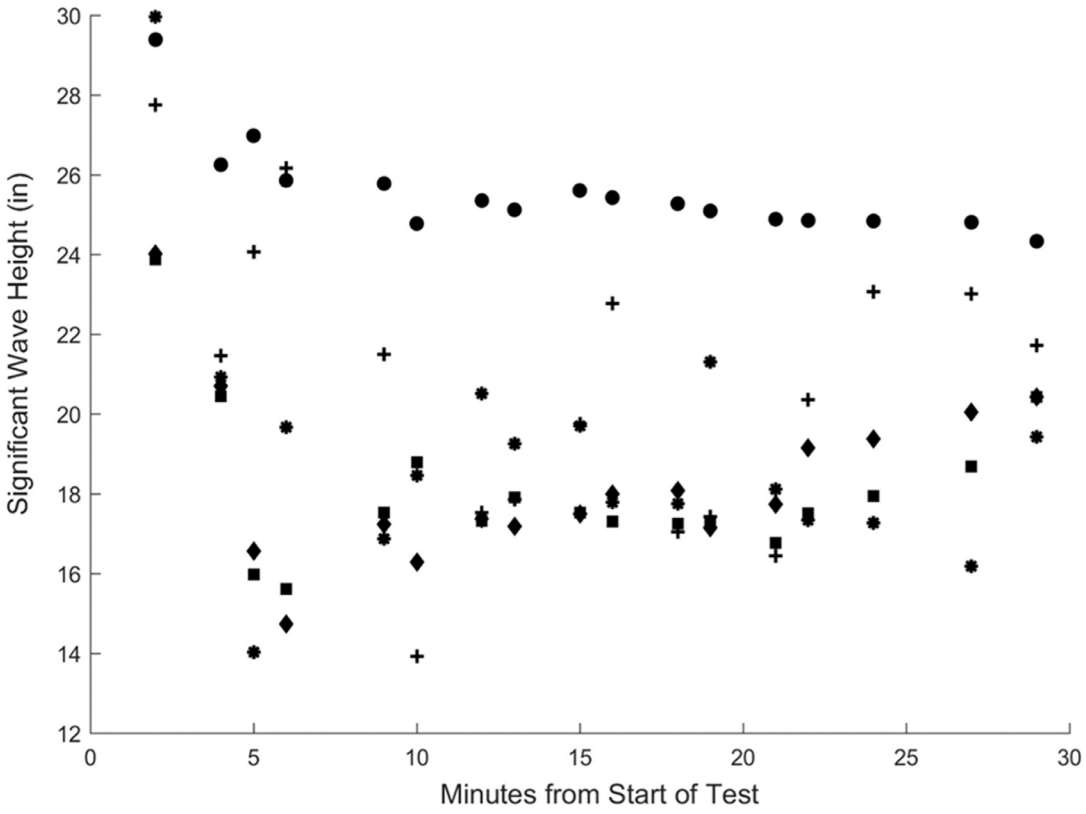

Fig. 6. Varied significant wave height (H_{m0}) due to complex wave fields during Test 2. This plot shows the significant wave height (H_{m0}) calculation for the WCM buoy, the WCM mounted to the skimmer, and all three Banner locations for Test 2. Here, the Buoy is represented by the crosses, the skimmer is represented by the stars, the main bridge Banner is represented by the dots, the west auxiliary bridge Banner is represented by the squares, and the east auxiliary bridge Banner is represented by the diamonds. Here it can be seen that there is variation in the significant wave height due to location in the tank.

torically calculated as the average of the highest third of the wave heights and denoted $H_{1/3}$. Significant wave height can also be defined as four times the standard deviation of the wave surface or four times the square root of the zeroth-order moment of the wave spectrum, denoted H_{m0}. Both calculation methods are valid, and generally differ only slightly.

The MATLAB program used at Ohmsett calculates the significant wave height using $H_{1/3}$ while the WCM reports significant wave height using H_{m0}. The Ohmsett calculation removes spikes that are over the maximum variation amplitude, then sorts the peak-to-trough amplitudes and finally calculates the mean of the top third of the data.

We expected some difference between the raw data from the WCM and the raw data from the Banner U-Gauge QT50U series transducer used by Ohmsett [28]. Not only does the Banner transducer collect readings at a different frequency, but these readings are manipulated using $H_{1/3}$ to calculate wave height, while the WCM is set to use H_{m0}. To compensate for some of these inconsistencies, we analyzed the Ohmsett data using the statistical algorithms in WAFO to calculate H_{m0}, providing some normalization between the two data sets. We also noted variation between raw data from the WCM and raw data from the Ohmsett Banners due to spatial differences in the locations of the devices. The reflections of the waves from the sides of the tank created complex wave field at different locations, so we were careful to use the Banner readings closest to the WCMs.

Fig. 6 shows the significant wave height (H_{m0}) calculation for the WCM buoy, the WCM mounted to the skimmer, and all three Banner locations for Test 2. In the figure, the buoy data is represented by crosses, the skimmer data is represented by stars, the main bridge Banner data is represented by circles, the west auxiliary bridge Banner data is represented by squares, and the east auxiliary bridge Banner data is represented by diamonds. Fig. 6 illustrates the variation in significant wave height due to the location of each data collection device.

Fig. 7 shows the significant wave height results from the skimmer for Test 19. Similar plots for each test and each Banner location can be found in the appendix of [27]. We used the raw data from the east Banner transducer on the auxiliary bridge since it was physically closest to the skimmer during testing. The crosses represent the significant wave heights (H_{m0}) calculated using the WCM data, while the triangles represent the significant wave height calculated statistically (H_{m0}) using the Banner data. The circles show the wave heights ($H_{1/3}$) calculated using the algorithm from Ohmsett. We found that calculating the H_{m0} wave height produces a result on average 3.5 inches higher than the wave height generated using $H_{1/3}$ in code from Ohmsett. The rest of our analysis uses the significant wave heights (H_{m0}) calculated

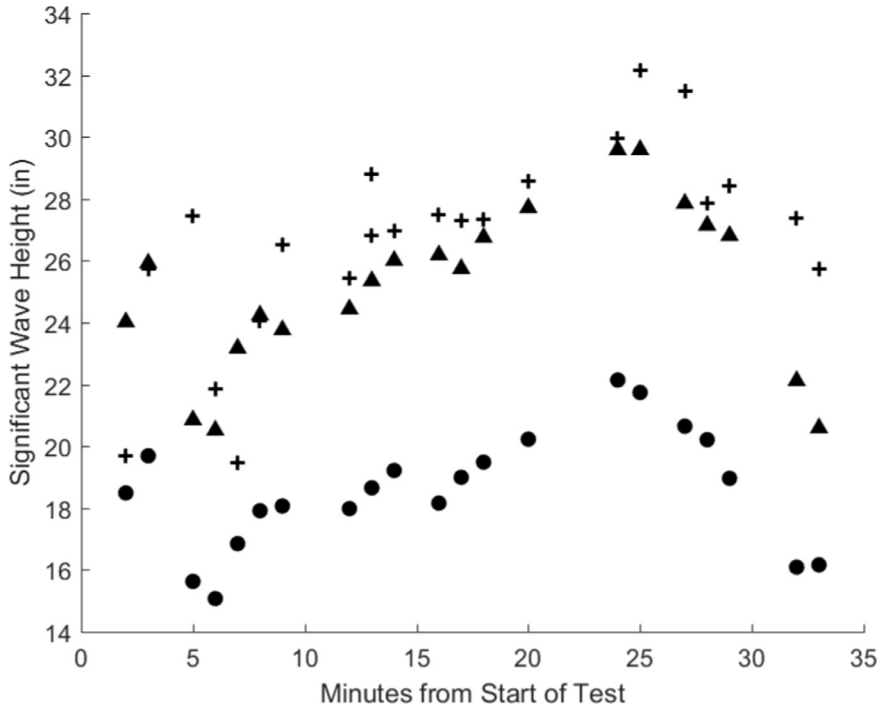

Fig. 7. Significant wave height results from the skimmer for Test 19. This plot shows the significant wave heights for Test 19. The plus signs indicate the significant wave height (H_{m0}) calculated statistically using the raw data from the WCM. The triangles represent the significant wave height (H_{m0}) calculated statistically using a segment of time corresponding to the WCM data from the raw Banner data. The dots represent the wave heights calculated using the average of the top third wave height from the same segments ($H_{1/3}$). Each data point represents a calculation of the significant wave height from approximately 60 s of raw data.

using the statistical algorithm from the east Banner on the auxiliary bridge.

Fig. 8 shows the difference between the significant wave heights calculated using the WCM data and the Banner data for Test 19. For this test, all WCM results are within the 4-inch performance objective with the exception of a few outliers. Plots showing the H_{m0} significant wave height for each test and Banner location are in the appendix of [27].

We have used the Banner data as the gold standard for comparing our results. The Banner itself has a declared measurement uncertainty of 0.2%, which results in approximately ±0.1 inch for the wave heights that were generated. For the measurement distances in use at Ohmsett, the ultrasonic beam spot size of the Banner device is between one and two feet in diameter, which could introduce additional uncertainty under certain wave conditions, though we did not consider this an issue for our tests. There is, however, some amount of uncertainty in the way we partitioned the raw data from Ohmsett. To segment the data, we identified a minute of data collected by the WCM using the timestamp of the data file. We located that minute, plus and minus 10 s, in the raw data file from Ohmsett.

Table 2 shows the mean differences for all the tests for each Banner. On average, the WCM attached on the skimmer was 2.7 inches higher and the buoy 1.3 inches higher than the significant wave height calculated statistically using the raw data from the east auxiliary bridge Banner.

Table 2
Mean differences for all tests for each banner.

	Mean difference (inches)		
	From main bridge Banner	From west aux bridge Banner	From east aux bridge Banner
Skimmer	3.3	3.5	2.7
Buoy	2.7	2.5	1.3

Fig. 9 shows the mean and standard deviation of the difference between the significant wave height from the WCM mounted on the skimmer and the east auxiliary bridge Banner data for each test. Differences between WCM data and data from the other Banners are in the appendix of [27].

Fig. 10 shows the mean and standard deviation of the difference between the significant wave height from the WCM Buoy and the east auxiliary bridge banner data for each test. In both Figs. 10 and 11, the mean of a test is represented by the circle and the whiskers are the standard deviation of that test. In all but a few cases, the WCM data and the Banner data were within 4 inches of each other.

Again, it is important to note the spatial differences in the locations of the devices and Banner measurement locations. The reflections of the waves from the sides of the tank create a complex wave field at different locations throughout the wave tank, where each point in the tank is unique and

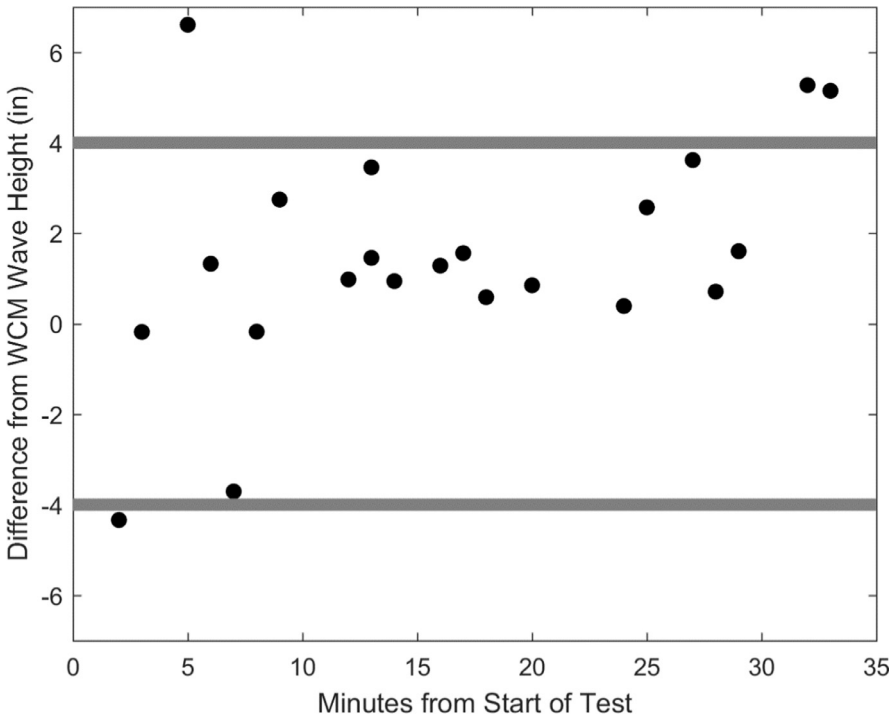

Fig. 8. Test 19 WCM on skimmer versus aux East Banner. This plot shows the difference of the significant wave heights calculated for Test 19. The plus signs indicate the difference between the significant wave height calculated statistically using the raw data from the WCM and the significant wave height calculated statistically using a segment of time corresponding to the WCM data from the raw Banner data. Each data point represents a calculation from approximately 60 s of raw data.

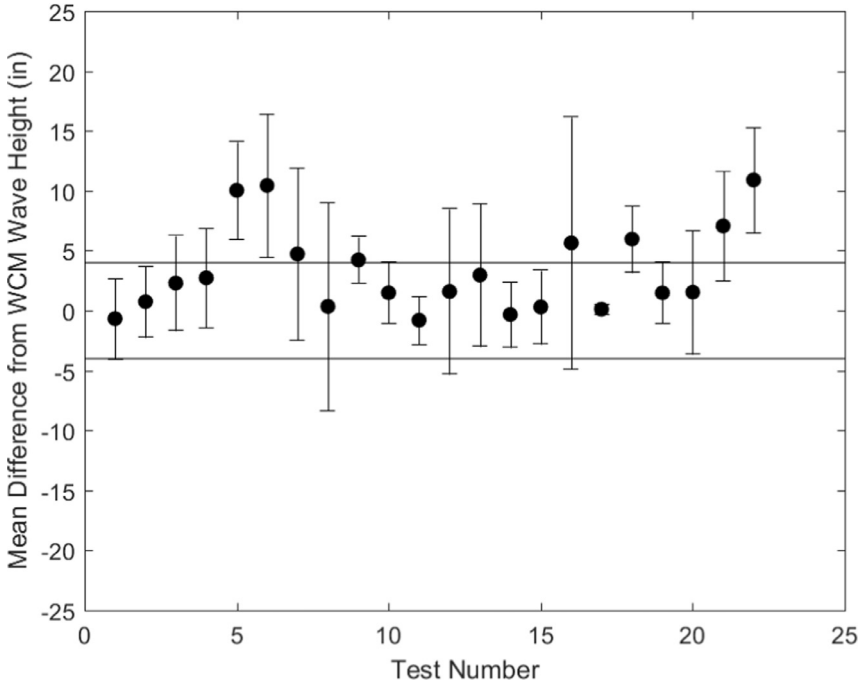

Fig. 9. WCM on skimmer mean and standard deviation by test. This plot shows the mean and standard deviation of differences in significant wave height for each test using the WCM attached to the skimmer. Each data point represents the mean of the difference between the significant wave height calculated statistically using the raw data from the WCM and the significant wave height calculated statistically using a segment of time corresponding to the WCM data from the raw Banner data for each test.

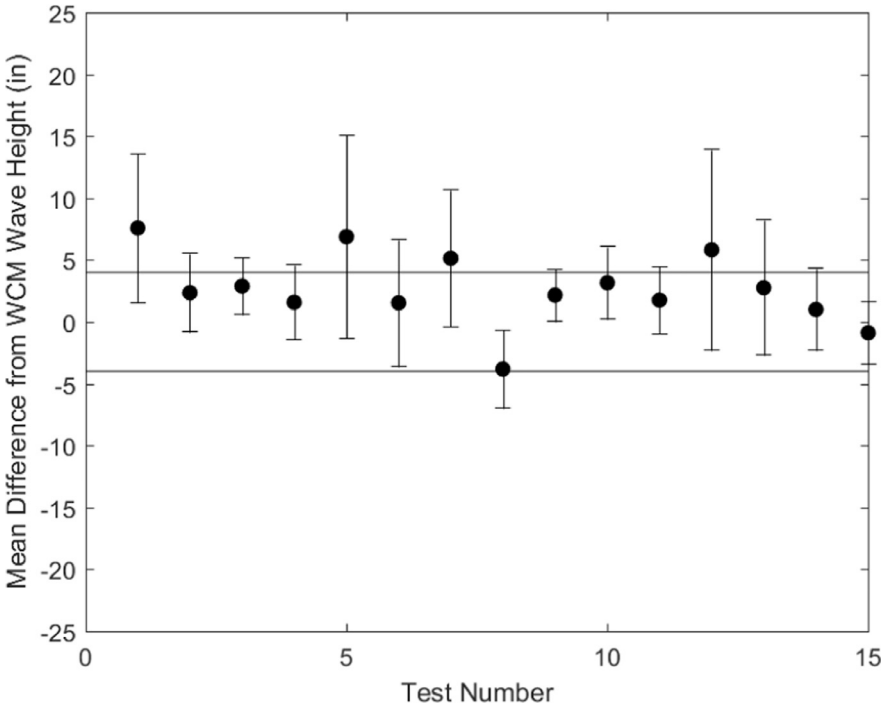

Fig. 10. WCM-Buoy mean and standard deviation by test. This plot shows the mean and standard deviation of differences of the significant wave height for each test using the WCM Buoy. Each data point represents the mean of the difference between the significant wave height calculated statistically using the raw data from the WCM and the significant wave height calculated statistically using a segment of time corresponding to the WCM data from the raw Banner data for each test.

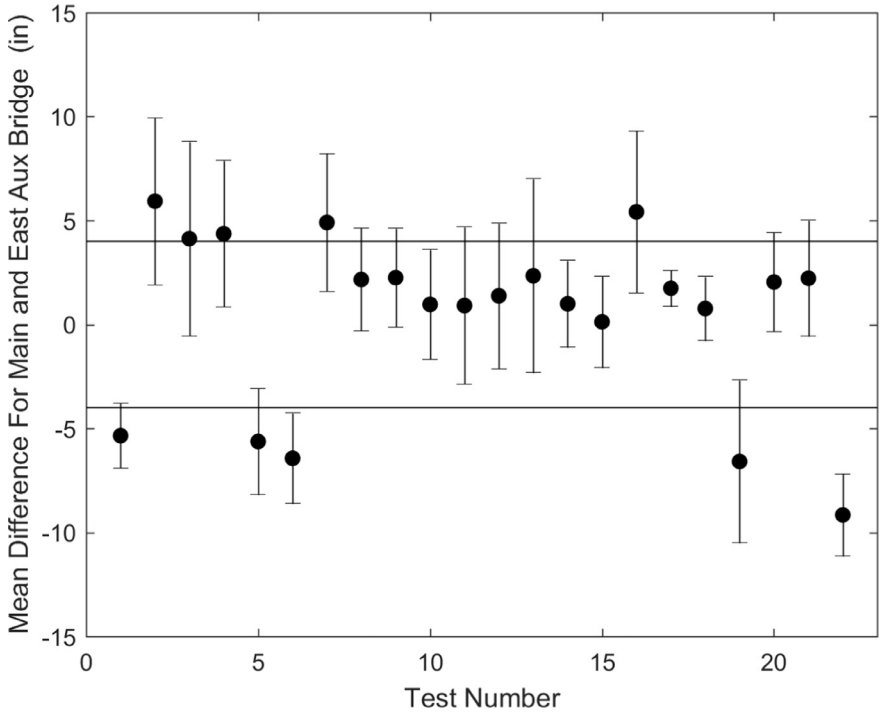

Fig. 11. Mean difference of main bridge Banner versus east aux bridge Banner. This plot shows the mean and standard deviation of differences of the significant wave height for each test between the main bridge Banner and the east auxiliary bridge Banner. Each data point represents the mean of the difference between the significant wave height calculated statistically using 80-s segments of the raw Banner data from Ohmsett. While there is small measurement error in the wave heights being measured by the Banner devices, there is a measurement uncertainty in the wave height due to the location of the device collecting data. This is due to the complex wave field generated in the tank.

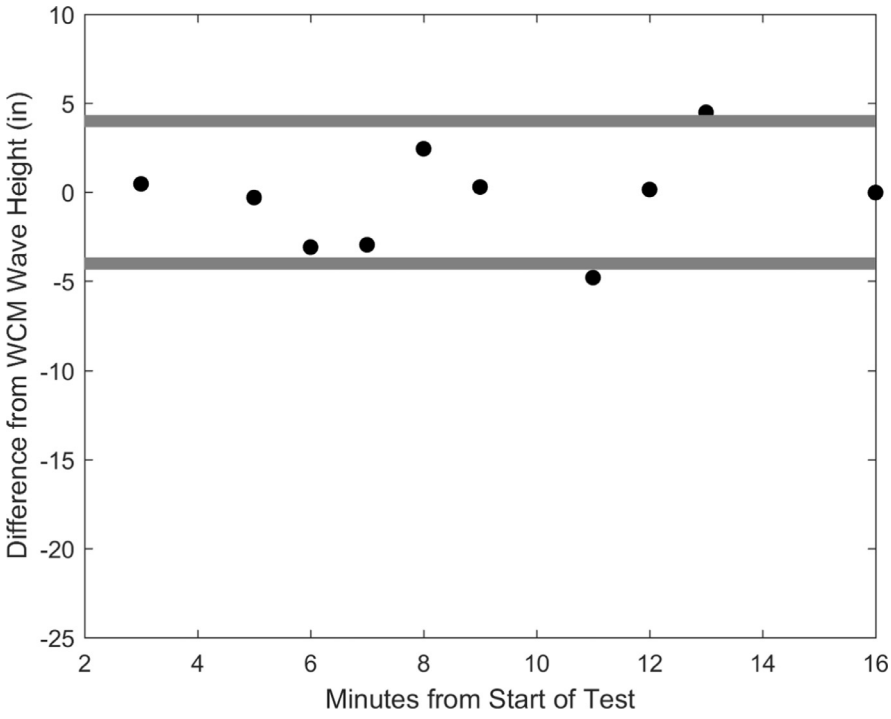

Fig. 12. Difference between the WCM and the east auxiliary bridge Banner significant wave height calculations for Test 14.

experiences different wave conditions. To demonstrate this, Fig. 11 compares the main bridge Banner sensor to the east auxiliary bridge Banner sensor. We observe several outliners and large standard deviations between the two Banner sensors on a number of tests. A comparison of the Banners is provided in the appendix of [27].

We collected raw data for one-minute at a time, with each test averaging 14 of these one-minute rounds of data collection. The mean was computed by finding the difference between the significant wave height of the WCM and the Banner data for a given minute in the test. We then calculated the means and standard deviations of these differences for each test. Test 14 and Test 8 have similar mean differences between the WCM and the east auxiliary bridge Banner at 0.3 inches but have large differences in the standard deviation, where the standard deviation for Test 14 is 2.7 inches and for Test 8 is 8.7 inches.

The plots in Figs. 12 and 13 explain this notable difference. Fig. 12 shows the plot of the difference between the WCM and the east auxiliary bridge Banner significant wave height calculations for Test 14. Fig. 13 shows the plot of the difference between the WCM and the east auxiliary bridge Banner significant wave height calculations for Test 8. From these results it can be seen that there was little variation in the significant wave height difference in Test 14, while Test 8 had a few outliers that increased the standard deviation.

4. Discussion of results

We used enhanced GRID and GRIDSAT tags, called wave characterization modules, to equip and test commercially available mechanical skimming units for wave characterization with an accuracy of about 4 inches. We mounted several WCMs and WCM-Sats on a weir skimmer along with a free-floating WCM-Buoy and successfully tested the system through various wave types and under conditions such as sinusoidal waves and harbor chop. Even with devices coated in crude oil and while towing the skimmer through waves, the system maintained successful operation and data communication. On average, data from the WCM attached to the skimmer was 2.7 inches higher and that from the buoy was 1.3 inches higher than the significant wave height calculated statistically using the raw data from the Ohmsett Banner. The accuracy of our devices throughout all wave types and testing conditions remained within our 4-inch performance objective.

For both skimmer and buoy, the mean values furthest from the performance objective were calculated for the waves created by the 18-inch stroke and 18 CPM setting of the wave generator. This creates a large sinusoidal wave with a significant wave height of approximately 22 inches. We believe the discrepancy between the wave heights is due to the artificial regularity of the waves in the tank. We collected training data in open water under complex conditions using both the buoy and a mockup skimmer. The open water conditions were deep-water waves with a water depth of approximately 20 feet, while the water depth at Ohmsett was 8 feet. Except in the choppy conditions, the wave tank produced sinusoidal waves with all of the energy moving in one direction. This created more lateral motion of the skimmer than did the complex open waves. Since we calculated wave height using the scalar magnitude of the x-, y- and z-axes, this lateral motion influenced the wave height calculation.

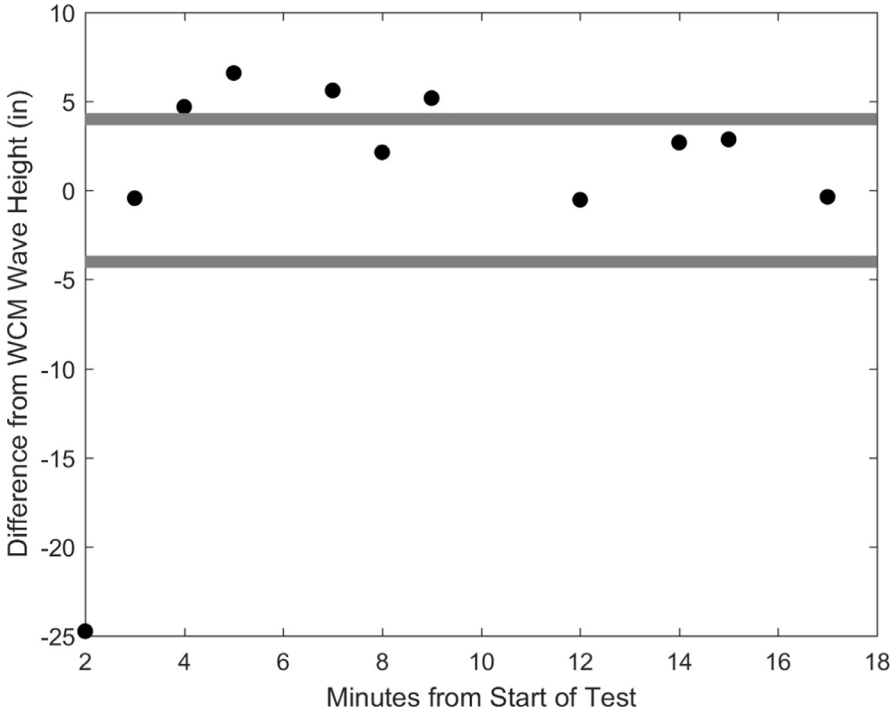

Fig. 13. Difference between the WCM and the east auxiliary bridge banner significant wave height calculations for Test 8. The data point at the start of the test highlights the potential discrepancies when the WCM and Banner are measuring different parts of a transient wave field developing in the tank.

The variation observed by Ohmsett in the calculated $H_{1/3}$ and the height of a single wave is typically around 10–40 percent, and in general longer periods show a larger difference. In addition to interference from reflections, constructive and deconstructive interference, etc., wavelengths greater than twice the water depth (8 feet for the Ohmsett tank) experience friction on the bottom of the basin, which influences the wave speed and profile of the waves. Harbor chop waves also sometimes have "hot spots" and can create higher values and greater variances between Banner measurement locations during a test run. According to Ohmsett staff, hot spots are likely due to the constructive/destructive interference of the waves. For example, Test 6 (Stroke 18, CPM 18) had a significant wave height difference between bridge Banner sensors of more than 7 inches for the same 1-minute time window. This large variance accounts for some of the large standard deviations and averages seen from the skimmer-mounted WCM and WCM-Buoy, which were positioned between the main, east, and west auxiliary bridge Banner sensors.

We conclude that the WCM, WCM-Sat, and WCM-Buoy performed well and were able to accurately report localized wave conditions. As the variation observed between the main bridge Banner and auxiliary bridge Banner sensors show, complex wave fields sometimes create very localized conditions. Our wave characterization modules demonstrate why localized sensors on skimmers and around recovery areas are critical in making informed decisions because other methods to access wave-field characteristics will have an uncertainty due to spatial variations in the waves, even if the measurement is nearby. Future work will increase the technology readiness level of the WCMs for use in follow-on testing during oil recovery exercises and emergencies.

5. Conclusion

We developed a system that characterizes ocean waves, leveraging an existing technology with the sensors and software needed to measure wave characteristics. Testing at Ohmsett showed an accuracy of about 4 inches when the system was deployed in a variety of wave types and under a range of conditions. Successful satellite communication of data to the cloud and GIS user interface as well as a user-friendly mobile application for local viewing of wave characteristics for enhanced quantitative situational awareness was simultaneously demonstrated [27]. Both the WCM-Sat and WCM-Buoy integrate a satellite modem for global coverage and reliable reporting of time, location, and wave information via a cloud-based solution to ingest and display the wave data on an Internet browser that has an accessible and easy-to-use GIS interface. This creates a common operating picture for stakeholders and provides actionable intelligence at local and regional levels. Finally, we created a user-friendly operator interface for skimmer operators. All three devices, WCM, WCM-Sat, and WCM-Buoy, have an integrated mesh network radio for device-to-device communication and a WiFi module for direct communication to a local user in real time, reporting wave characterization data. A tablet application dashboard is used to retrieve and display wave characterization reports to aid in situational awareness for skimmer operators.

Acknowledgments

This work was supported by the Bureau of Safety and Environmental Enforcement (BSEE), U.S. Department of the Interior, Washington, D.C., under Contract: E16PC00015: Equip GRID and GRIDSAT Tags with Accelerometers to Measure Ocean Waves [27]. Principal Investigator, B. Schreib, AECOM.

The authors thank Ben Schreib, Manuel Sanchez, Stephen Sporik, and Austin Vershel of AECOM, Sam McClintock and Ted Hale of Midstream Technology, and Navid Yazdi and Siva Aduri of Evigia Systems.

Contributions

E. Skinner and M. Rooney collected the laboratory data. E. Skinner collected the Albermarle Sound data and led the effort to collect the WCM data at Ohmsett. M. Hinders guided the experimental design and data processing algorithm selection. Data analysis was performed by E. Skinner and M. Rooney, advised by M. Hinders. All authors contributed to the preparation of the manuscript.

Competing interests statement

E. Skinner is currently Lead Scientist at Midstream Technology in Williamsburg, VA.

References

[1] D. Dave, A. Ghaly, Am. J. Environ. Sci. 7 (5) (2011) 423–440.
[2] N.P. Ventikos, E. Vergetis, H.N. Psaraftis, G. Triantafyllou, J. Hazard. Mater. 107 (1–2) (2004) 51–58, doi:10.1016/j.jhazmat.2003.11.009.
[3] D.P. Prendergast, P.M. Gschwend, J. Clean. Product. 78 (2014) 233–242, doi:10.1016/j.jclepro.2014.04.054.
[4] G. Johnson, C. Grayson, A. Stromlund, in: Proceedings of the International Oil Spill Conference, 2017, May 2017, pp. 1382–1402.
[5] H.S. Holt, B.R. Frost, in: Proceedings of the International Oil Spill Conference, 2017, May 2017, pp. 1403–1416.
[6] http://www.metocean.com/sites/default/files/files/products/pdfs/isphere_brochure_0.pdf.
[7] http://www.oceanor.no/seawatch/buoys-and-sensor/.
[8] http://www.datawell.nl/Products/Buoys.aspx.
[9] http://axystechnologies.com/products/triaxys-mini-directional-wave-buoy/ See also: http://axystechnologies.com/wp-content/uploads/2016/09/TRIAXYS-g3-Wave-Sensor-Validation-whitepaper.pdf.
[10] http://www.datawell.nl/Portals/0/Documents/Brochures/datawell_brochure_dwr-g4_b-06-09.pdf.
[11] C.O. Collins, B. Lund, T. Waseda, et al., Ocean Dyn. 64 (6) (2014) 895–904, doi:10.1007/s10236-014-0732-7.
[12] C.O. Collins, B. Lund, R.J. Ramos, W.M. Drennan, H.C. Graber, J. Atmosp. Ocean. Technol. 31 (10) (2014) 2309–2329.
[13] Y. Hirakawa, T. Takayama, T. Hirayama, H. Susaki, in: Proceedings of the OCEANS 2016 MTS/IEEE Monterey, Monterey, CA, 2016, pp. 1–4, doi:10.1109/OCEANS.2016.7761337.
[14] M.C. Marimon, G. Tangonan, N.J. Libatique, K. Sugimoto, IEEE Syst. J. 9 (1) (2015) 292–302, doi:10.1109/JSYST.2013.2284102.
[15] F. Yu, X. Hu, S. Dong, et al., J. Marine Sci. Technol. (2017) 1–3, doi:10.1007/s00773-017-0472-8.
[16] H. Senga, N. Kato, H. Suzuki, et al., J. Marine Sci. Technol. 19 (1) (2014) 90–102, doi:10.1007/s00773-013-0233-2.
[17] Schreib et al. (2015) GEO – REFERENCING IDENTIFICATION (GRID) TAG, Final Report for Bureau of Safety and Environmental Enforcement (BSEE) Contract: E14PC0002, https://www.bsee.gov/sites/bsee.gov/files/osrr-oil-spill-response-research//1050aa.pdf.
[18] CDIP (Coastal Data Information Program). "Wave measurement." https://cdip.ucsd.edu/?nav=documents&sub=index&xitem=waves. Retrieved November 28, 2016.
[19] S.R. Massel, Advanced Series on Ocean Engineering, 36, World Scientific Publishing Co. Pte. Ltd., 2013 ISBN-978-981-4460-10-1.
[20] S. Pond, G. Pickard, Introductory Dynamic Oceanography, second ed., Pergamon Press, 1983 ISBN-0-08-028729-8.
[21] V.M. Kamenkovich, Fundamentals of Ocean Dynamics, Elsevier Scientific Publishing Company, 1977 ISBN-0-444-41546-7.
[22] J.B. Zirker, The Science of Ocean Waves Ripples, Tsunamis, and Stormy Seas, The Johns Hopkins University Press, 2013 ISBN-978-1-4214-1078-4.
[23] O.M. Phillips, The Dynamics of the Upper Ocean, Cambridge University Press, 1977 ISBN-0-521-21421-1.
[24] *Waves*, Tides and Shallow – Water Processes, 1989, Pergamon Press in association with The Open University, ISBN-0-08-036372-5.
[25] P.A. Brodtkorb, P. Johannesson, G. Lindgren, I. Rychlik, J. Rydén, E. Sjö, "WAFO – a Matlab toolbox for analysis of random waves and loads." Proceedings of the Tenth International Offshore and Polar Engineering Conference, Seattle, USA, Vol. III, pp. 343350, (2000) See also http://www.maths.lth.se/matstat/wafo/documentation/wafotutor25.pdf.
[26] http://www.publications.usace.army.mil/Portals/76/Publications/EngineerManuals/EM_1110-2-1100_Part-02.pdf?ver=2016-02-11-153511-290.
[27] Schreib et al. Equip GRID and GRIDSAT Tags with Accelerometers to Measure Ocean Waves Wave Characterization Modules (WCMs). Final Report for Bureau of Safety and Environmental Enforcement (BSEE) Contract: E16PC00015. (2017)
[28] "Item Detail QT50U Series 8M Range Chemical Resistant Ultrasonic Sensor." https://www.bannerengineering.com/us/en/products/part.02726.html . Retrieved November 7, 2017.
[29] https://www.ohmsett.com/facility.html.
[30] http://www.desmi.com/userfiles/file/manuals/oil%20spill%20response/m-terminator.pdf.